1 **Title:** Single-nucleus transcriptomics reveals time-dependent and cell-type-specific effects of

2 psilocybin on gene expression

3

4 **Authors:** Clara Liao[1,2,#], Ethan O'Farrell[3,4,#], Yaman Qalieh[3,4], Neil K. Savalia[1,2,5], Matthew J.

5 Girgenti[6,7], Kenneth Y. Kwan[3,4,*], and Alex C. Kwan[1,8,*]

6

7 [1]Meinig School of Biomedical Engineering, Cornell University, Ithaca, NY 14853, USA

8 [2]Interdepartmental Neuroscience Program, Yale University School of Medicine, New Haven, CT

9 06511, USA

10 [3]Michigan Neuroscience Institute, University of Michigan, Ann Arbor, MI 48109, USA

11 [4]Department of Human Genetics, University of Michigan, Ann Arbor, MI 48109, USA

12 [5]Medical Scientist Training Program, Yale University School of Medicine, New Haven,

13 Connecticut, 06511, USA

14 [6]Department of Psychiatry, Yale School of Medicine, New Haven, CT 06511, USA

15 [7]Clinical Neuroscience Division, National Center for Posttraumatic Stress Disorder, Veterans

16 Affairs Connecticut Healthcare System, West Haven, CT 06516, USA

17 [8]Department of Psychiatry, Weill Cornell Medicine, New York, NY 10065, USA

18

19 [#]These authors contributed equally to the work

20 *Correspondence to Kenneth Y. Kwan (kykwan@umich.edu) and Alex C. Kwan

21 (alex.kwan@cornell.edu)

22

23 **Keywords:**

24 Psychedelic, ketamine, frontal cortex, pyramidal cells, inhibitory neurons, RNA sequencing

25

ABSTRACT

There is growing interest to investigate classic psychedelics as potential therapeutics for mental illnesses. Previous studies have demonstrated that one dose of psilocybin leads to persisting neural and behavioral changes. The durability of psilocybin's effects suggests that there are likely alterations of gene expression at the transcriptional level. In this study, we performed single-nucleus RNA sequencing of the dorsal medial frontal cortex of male and female mice. Samples were collected at 1, 2, 4, 24, or 72 hours after psilocybin or ketamine administration and from control animals. At baseline, major excitatory and GABAergic cell types selectively express particular serotonin receptor transcripts. The psilocybin-evoked differentially expressed genes in excitatory neurons were involved in synaptic plasticity, which were distinct from genes enriched in GABAergic neurons that contribute to mitochondrial function and cellular metabolism. The effect of psilocybin on gene expression was time-dependent, including an early phase at 1-2 hours followed by a late phase at 72 hours of transcriptional response after administration. Ketamine administration produced transcriptional changes that show a high degree of correlation to those induced by psilocybin. Collectively, the results reveal that psilocybin produces time-dependent and cell-type specific changes in gene expression in the medial frontal cortex, which may underpin the drug's long-term effects on neural circuits and behavior.

INTRODUCTION

Psilocybin is a serotonergic psychedelic that has shown promise as a potential therapeutic for mental health conditions. Data from several clinical trials indicate that psilocybin with psychological support can relieve symptoms in patients with major depressive disorder or treatment-resistant depression[1, 2, 3, 4, 5]. Although the neurobiological basis for the therapeutic effects is not understood, there is growing evidence that the antidepressant effect may relate to the drug-evoked structural neural plasticity in the prefrontal cortex[6]. The plasticity-promoting effect of psilocybin and its active metabolite psilocin was demonstrated with cultured cortical neurons, where the application of psilocin induced dendritic outgrowth and spinogenesis[7]. Moreover, in live mice, psilocybin administration elevates the density of dendritic spines in the mouse medial frontal cortex, an effect that persists for over a month[8, 9]. Therefore, studies in humans and model systems suggest psilocybin can induce enduring effects on neuronal connectivity and behavior.

Long-lasting modifications to synaptic connections and behavior require changes in gene expression[10, 11]. Indeed, previous studies of mRNA transcript and protein levels identified differential expression of genes for synaptic function, glutamate receptor signaling, and immune response in the neocortex after a single dose of a classic psychedelic such as 2,5-dimethoxy-4-iodoamphetamine (DOI)[12, 13, 14, 15], lysergic acid diethylamide (LSD)[12, 16], 5-methoxy-N,N-dimethyltryptamine (5-MeO-DMT)[17], or psilocybin[15, 18, 19]. Although these results demonstrated transcriptional alterations after drug exposure, the early studies relied on methods such as quantitative PCR and microarrays, which were limited by their focus on preselected candidate genes. A genome-wide transcriptomic investigation can yield novel insights, as exemplified by recent studies of transcriptional responses to drugs such as cocaine[20, 21, 22], heroin[23], fentanyl[24], DOI[14], MDMA[25], ketamine and imipramine[26], as well as in mouse models of chronic stress[27, 28] and early life stress[29, 30].

In addition to the goal of sequencing the transcriptome, understanding the temporal dynamics of the transcriptional response is also important. In humans, the oral administration of psilocybin induces subjective effects on perception and emotion within 30 minutes[31, 32]. Peak subjective effects for some individuals arrive as early as 60 minutes, coinciding with peak plasma psilocin levels[33] and pronounced changes in brain functional connectivity[34]. The subjective effects subside in 3 – 6 hours[32], because of rapid clearance with an elimination half-life of 3 hours[35]. Long after the subjective effects wear off, therapeutic effects for major depression can be

80   detected with an onset at 2 – 8 days[1, 4], and persist for at least 6 weeks after the initial

81   administration[4]. Although reverse translation of this time course to rodents is inexact, psilocybin

82   produces likewise acute effects in mice within a couple hours, including head-twitch responses[8,

83   36], ultrasonic vocalizations[37], and cognitive flexibility[38]. These are followed in subsequent days

84   by changes in behavioral assays such as learned helplessness[8, 9], forced swim[39], tail

85   suspension[9], sucrose preference[40, 41], fear extinction[42], and social reward learning[25]. Therefore,

86   efforts to understand psilocybin-evoked changes in gene expression should consider time as a

87   key parameter.

88

89   With these goals in mind, we designed a study to perform single-nucleus RNA sequencing

90   (snRNA-seq) to determine the transcriptomic changes in the dorsal medial frontal cortex of male

91   and female mice after psilocybin administration. To capture both acute and long-term changes,

92   we collected tissues at 1, 2, 4, 24, and 72 hours after drug exposure, as well as from control

93   animals. We delineated differentially expressed genes (DEGs) due to psilocybin administration

94   in excitatory and GABAergic cell types. For excitatory neurons, our results show that psilocybin

95   leads to an overrepresentation of genes linked to synaptic plasticity. By contrast, GABAergic

96   interneurons showed an enrichment in biological processes associated with mitochondrial

97   function and cellular metabolism. Temporally, we identified two waves of elevated transcriptional

98   responses: an initial phase at 1-2 hours and a late phase at 72 hours after psilocybin

99   administration. Collectively, the results reveal cell-type-specific and time-dependent changes to

100   the transcriptional landscape in the mouse medial frontal cortex after a single dose of psilocybin.

101

102   **RESULTS**

103

104   **Single-nucleus RNA sequencing of the mouse medial frontal cortex at various timepoints**

105   **after a single dose of psilocybin**

106   In this study, we focus on the mouse dorsal medial frontal cortex, which encompasses the

107   anterior cingulate cortex (ACAd) and the premotor cortex (medial MOs). This region is important

108   for the drug action of psilocybin and ketamine, showing robust c-Fos response[43] and structural

109   neural plasticity[8, 9] following psilocybin administration. We administered C57/BL6J mice with

110   psilocybin (1 mg/kg, i.p.), and then collected tissues corresponding to the dorsal medial frontal

111   cortex of both hemispheres via microdissection at 1, 2, 4, 24, or 72 hours after drug

112   administration (n = 20 animals; 2 male and 2 female for each time point; **Figure 1a**). Additionally,

113   we collected control tissues via the same method from animals that received no injection (n = 9

114   animals; 3 male and 6 female). The tissues were processed through nuclear dissociation, nuclei

115   sorting, and barcoding for snRNA-seq via the 10x Genomics Chromium Single Cell 3' v3

116   platform. We started with 145,593 cells that were sequenced at a mean depth of 9023±366

117   reads per cell for the psilocybin group, and 67,600 cells that were sequenced at a mean depth

118   of 8423±302 reads per cell for the controls. After removing cells that did not meet quality control

119   criteria (see **Methods**), our data set consisted of 122,685 cells for the psilocybin group (range =

120   18,944 – 31,443 single nuclei per time point; n = 17 animals) and 56,693 cells for the control
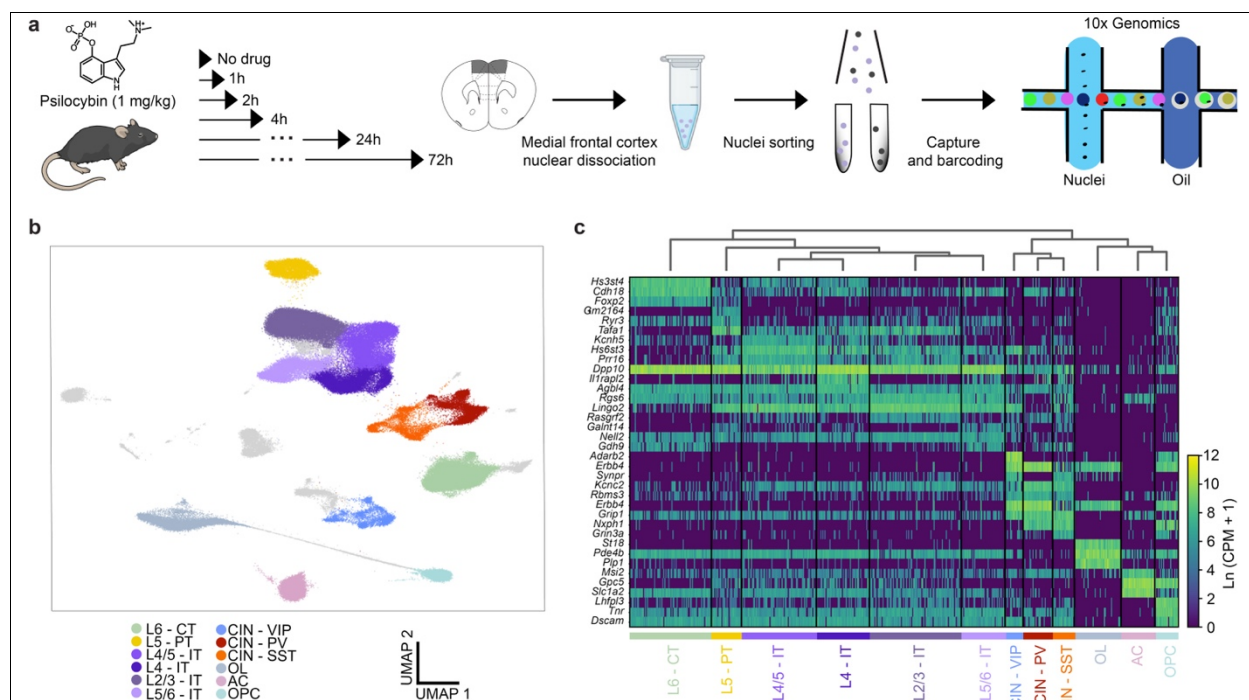
121   group (n = 8 animals).

122

Fig. 1: Single-nucleus RNA sequencing of mouse medial frontal cortex after psilocybin administration.
(a) Experimental workflow.
(b) UMAP representation of the snRNA-seq data set including 122,685 nuclei from psilocybin-treated mice (range = 18,944 – 31,443 nuclei per time point; n = 17 animals) and 56,693 nuclei from the control mice (n = 8 animals). Color denotes the cell-type cluster.
(c) Heatmap for the expression of cell-type-specific genes for the cell-type clusters. Dendrogram was generated by performing hierarchical clustering using expression profiles across all conditions. CPM, count per million.
L6-CT, layer 6 corticothalamic. L5-PT, layer 5 pyramidal tract. L4/5-IT, layer 4/5 intratelencephalic. L4-IT, layer 4 intratelencephalic. L2/3-IT, layer 2/3 intratelencephalic. L5/6-IT, layer 5/6 intratelencephalic. CIN-VIP, cortical vasointestinal peptide-expressing interneurons. CIN-PV, cortical parvalbumin-expressing interneurons. CIN-SST, cortical somatostatin-expressing interneurons. OL, oligodendrocytes. AC, astrocytes. OPC, oligodendrocyte progenitor cells.
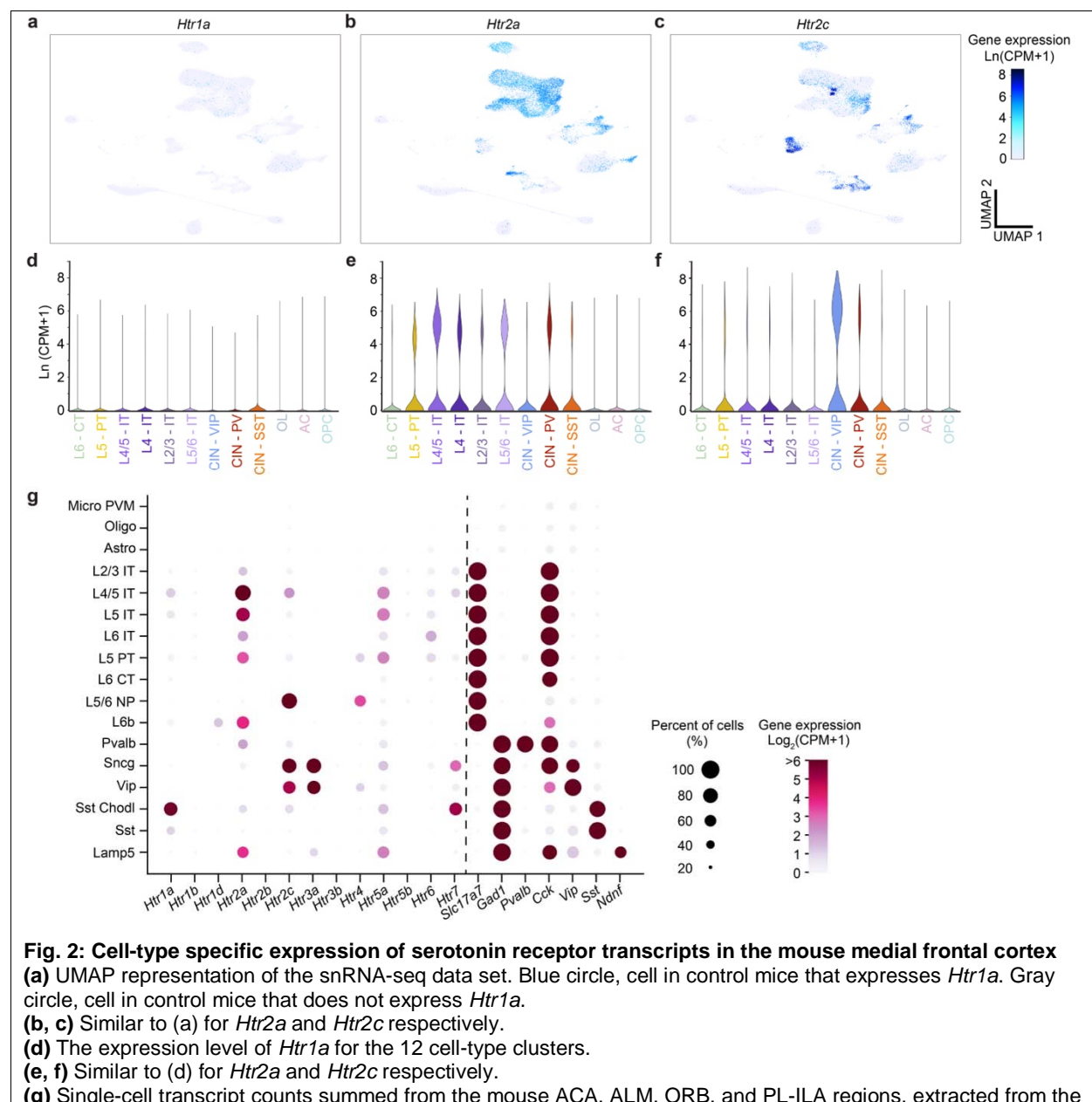
123

124   We segmented the cells into clusters by performing dimensionality reduction and then Leiden

125   clustering. Among all clusters, we focused on 12 clusters identified based on expression profiles

126   of established marker genes and annotated them with corresponding cell types (**Figure 1b, c**;

127   see **Methods**). The majority of cells were classified into one of these clusters, including 108,060

128   cells (88.13%) in the psilocybin group and 49,963 cells (88.08%) in the control group. The 12

129   clusters included 6 classes of excitatory neurons – layer 6 corticothalamic neurons (L6-CT;

130   number of cells per time point or control condition: 3952±750, 13.2% of all cells that met quality

131   control criteria), layer 5 pyramidal tract neurons (L5-PT; 1420±241, 4.8%), layer 4/5

132   intratelencephalic neurons (L4/5-IT; 3582±761 cells, 12.0%), layer 4 intratelencephalic neurons

133   (L4-IT; 2469±450, 8.3%), layer 2/3 intratelencephalic neurons (L2/3-IT; 4402±856, 15.0%), and

134   layer 5/6 intratelencephalic neurons (L5/6-IT; 2090±374, 7.0%), alongside 3 classes of

135   GABAergic neurons – vasoactive intestinal peptide-expressing interneurons (CIN-VIP; 853±134,

136   2.9%), parvalbumin-expressing interneurons (CIN-PV; 1425±234, 4.8%), and somatostatin-

137   expressing interneurons (CIN-SST; 1039±150, 3.5%), as well as 3 classes of non-neuronal cells

138   – oligodendrocytes (OL; 2179±626, 7.3%), astrocytes (AC; 1680±323, 5.6%), and

139   oligodendrocyte progenitor cells (OPC; 1156±220, 3.9%) (**Supplementary Table 1**). The same

140   cell-type clusters were detected in samples collected at different time points after psilocybin

141   administration and in controls (**Figure S1**).

142

143   **Cell-type specific expression of serotonin receptor transcripts in the mouse medial**

144   **frontal cortex**

145   Psilocin binds not only to the 5-HT$_{2A}$ receptor, but also to other serotonin receptor subtypes

146   expressed in the neocortex, including the 5-HT$_{1A}$ and 5-HT$_{2C}$ receptors[44, 45]. We visualized the

147   presence of the *Htr1a*, *Htr2a*, and *Htr2c* transcripts which encode the 5-HT$_{1A}$, 5-HT$_{2A}$, and 5-

148   HT$_{2C}$ receptors respectively in the control samples in our snRNA-seq data set (**Figure 2a – c**).

149   The distribution of the three transcripts clearly differed, prompting us to quantify how the

150   transcript levels vary across the 12 cell-type clusters (**Figure 2d – f**). To further support this

151   analysis and incorporate additional identified cell types, we also extracted publicly available

152   single-cell sequencing data from the Allen Institute[46], focusing on cells residing in the mouse

153   frontal cortex, including the ACA, ALM, ORB, and PL-ILA regions (**Figure 2g**). There was a

154   strong agreement between the two data sets. Many IT and PT excitatory neurons express a

155   high level of *Htr2a* as well as moderate amounts of *Htr1a* and *Htr2c*. Interestingly, there is also

156   an abundance of *Htr2a* transcripts in the deep-lying Layer 6b neurons, which are known for their

157   excitatory effects on apical dendrites and higher-order thalamus[47]. Unlike the excitatory neurons,

158   the expression pattern is more selective in the GABAergic cell subtypes. The three major

159   interneuron subtypes – CIN-PV, CIN-SST, and CIN-VIP – predominantly express only one of

160   the receptor transcripts: *Htr2a*, *Htr1a*, and *Htr2c* respectively. *Lamp5*-expressing interneurons,

161   which include the *Ndnf*-expressing neurogliaform cells[48], express *Htr2a*, with relatively minimal

162   expression of *Htr1a and Htr2c*. Finally, although serotonin receptors have been reported in

163   microglia[49, 50] and astrocytes[51], the current data suggest that the *Htr* transcript levels are

164   relatively low in the non-neuronal cell types. Altogether, these analyses reveal a highly selective

165   pattern for how serotonin receptors are expressed in cortical cell types. Because psilocin is a

166   non-selective serotonergic agonist that binds to a range of receptor subtypes, we anticipate that

167   the drug can directly influence the transcriptional programs of most major excitatory and

168   GABAergic cell types.

169

Fig. 2: Cell-type specific expression of serotonin receptor transcripts in the mouse medial frontal cortex
(a) UMAP representation of the snRNA-seq data set. Blue circle, cell in control mice that expresses *Htr1a*. Gray circle, cell in control mice that does not express *Htr1a*.
(b, c) Similar to (a) for *Htr2a* and *Htr2c* respectively.
(d) The expression level of *Htr1a* for the 12 cell-type clusters.
(e, f) Similar to (d) for *Htr2a* and *Htr2c* respectively.
(g) Single-cell transcript counts summed from the mouse ACA, ALM, ORB, and PL-ILA regions, extracted from the

SMART-Seq data set from Allen Institute. *Slc17a7* and *Gad1* are markers of excitatory and GABAergic neurons, respectively. *Pvalb*, *Cck*, *Vip*, *Sst*, and *Ndnf* are markers of subtypes of GABAergic neurons.

170

Psilocybin-induced transcriptional changes in frontal cortical excitatory neurons are involved in synaptic plasticity

173 To examine how psilocybin alters the broad transcriptomic landscape, we implemented

174 memento[52], an end-to-end framework that uses a hierarchical model for statistical analyses of

175 multidimensional sequencing data. This analysis showed that certain cell types had similar

176 patterns of transcriptionally responsive genes evoked by psilocybin (**Figure S2**). Informed by

177 this, we grouped L4/5-IT, L4-IT, L2/3-IT, L5/6-IT cell types together as IT neurons, and CIN-VIP,

178 CIN-PV, CIN-SST cell types together as cortical interneurons (CINs). The IT neurons and CINs

179 were compared to L5-PT neurons (PT neurons). This aggregation allowed us to proceed next to

180 identify DEGs with more cells in each group at each time point (PT: 1420±241 cells, range =

181 971–1415 for psilocybin and 2568 for control; IT: 12633±2430 cells, 7354–13102 and 24123;

182 CIN: 3318±516 cells, 2308–3415 and 5773).

183

184 To identify specific DEGs, we used pseudobulk analysis where sequence reads were summed

185 for each cell group and individual replicate. Differential expression analysis was performed

186 using edgeR[53]. Pseudobulk analysis has been shown to yield reliable quantifications with fewer

187 false positives[54, 55]. We first determined DEGs in the excitatory pyramidal neurons **(Figure 3a).**

188 For PT neurons, we detected a high number of DEGs (1698 with FDR < 0.05) at 1 hour after

189 psilocybin administration (**Figure 3b**). Psilocybin caused both upregulation and downregulation

190 at this 1-hour time point (57% and 43% respectively among DEGs). Subsequently, the drug's

191 effect on transcriptional activity waned precipitously with only 108, 103, and 14 DEGs detected

192 at 2, 4, and 24 hours after psilocybin administration. Intriguingly, the number of DEGs climbed

193 back to 822 at 72 hours after drug exposure (35% upregulated and 65% downregulated among

194 DEGs). A similar time course for DEGs was observed in IT neurons (**Figure 3b**). Psilocybin

195 evoked 3401 DEGs (FDR < 0.05) in IT neurons at the 1-hour time point (52% upregulated and

196 48% downregulated), which dropped to 887, 192, and 6 DEGs at the 2, 4, and 24-hour time

197 points, before rising to 2549 DEGs at the 72-hour time point (43% upregulated and 57%
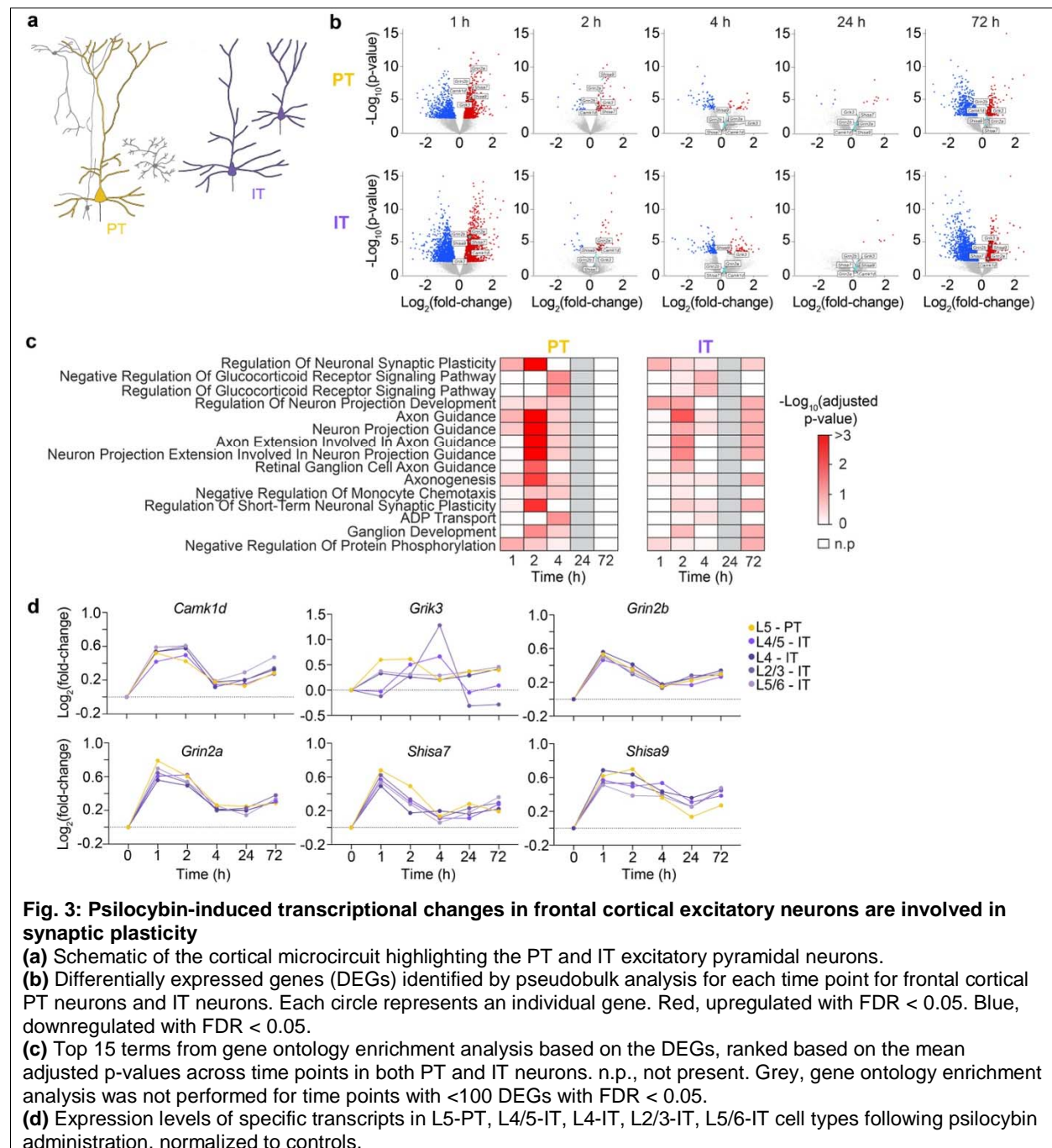
198 downregulated).

199

Fig. 3: Psilocybin-induced transcriptional changes in frontal cortical excitatory neurons are involved in synaptic plasticity

(a) Schematic of the cortical microcircuit highlighting the PT and IT excitatory pyramidal neurons.

(b) Differentially expressed genes (DEGs) identified by pseudobulk analysis for each time point for frontal cortical PT neurons and IT neurons. Each circle represents an individual gene. Red, upregulated with FDR < 0.05. Blue, downregulated with FDR < 0.05.

(c) Top 15 terms from gene ontology enrichment analysis based on the DEGs, ranked based on the mean adjusted p-values across time points in both PT and IT neurons. n.p., not present. Grey, gene ontology enrichment analysis was not performed for time points with <100 DEGs with FDR < 0.05.

(d) Expression levels of specific transcripts in L5-PT, L4/5-IT, L4-IT, L2/3-IT, L5/6-IT cell types following psilocybin administration, normalized to controls.

200

201   To gain insights into the functions of the psilocybin-induced transcriptional changes, we

202   performed gene ontology (GO) enrichment analysis for the DEGs identified in PT and IT

203   neurons at different time points. **Figure 3c** shows the top 15 overrepresented GO terms when

204   we considered the prevalence of each term averaged across all time points and for both

205   excitatory cell types. The top terms involve the regulation of glucocorticoid receptor signaling in

206   the brain and numerous processes related to synaptic plasticity and neuronal connectivity,
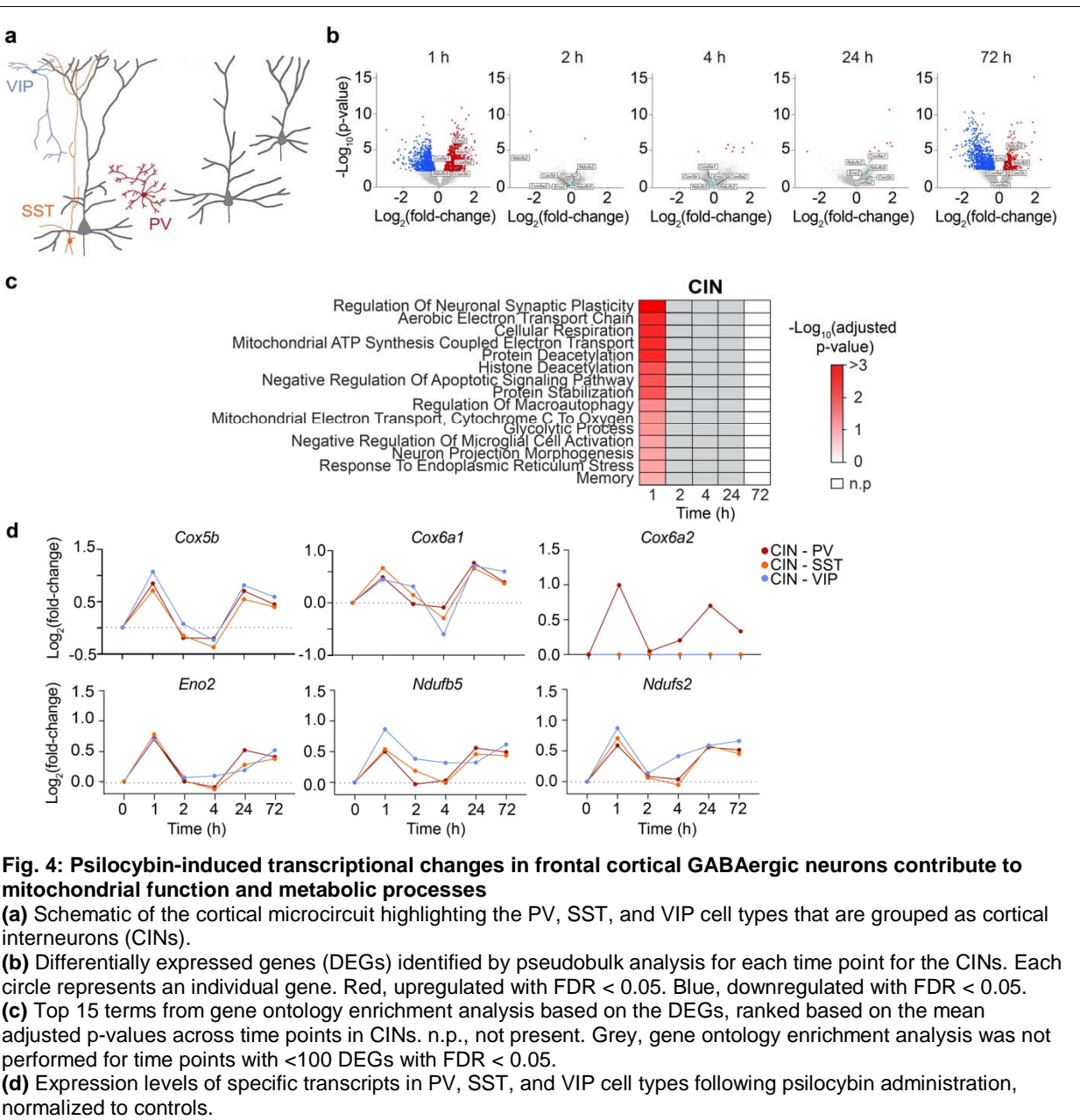
207 including the regulation of neuronal synaptic plasticity, regulation of neuron projection

208 development, axon guidance, neuron projection guidance, axon extension involved in axon

209 guidance, neuron projection extension involved in neuron projection guidance, axogenesis, and

210 regulation of short-term neuronal synaptic plasticity. The engagement of mechanisms included

211 in these terms was time-dependent (main effect of time: $P = 1.6 \times 10^{-12}$, main effect of cell type:

212 $P = 0.03$, two-way ANOVA with post-hoc pairwise statistics reported; **Supplementary Table 2**).

213

214 We visualized select upregulated genes that are part of the enriched pathways such as *Camk1d*,

215 *Grik3*, *Grin2b*, *Grin2a*, *Shisa9*, and *Shisa7* (mean $\log_2$(fold-change) = +0.351, +0.303, +0.393,

216 +0.312, +0.296, +0.446, respectively; **Figure 3d**). *Camk1d* is a member of the

217 calcium/calmodulin-dependent protein kinase 1 family that regulates dendritogenesis[56] and

218 NMDA receptor-mediated calcium elevation[57]. *Grik3*, *Grin2b*, and *Grin2a* encode subunits of

219 ionotropic glutamate receptors[58]. *Shisa9* and *Shisa7* encode AMPA receptor-associated

220 proteins that modulate AMPA channel kinetics and receptor trafficking[59, 60]. These

221 transcriptionally upregulated genes are expected to contribute to the regulation of excitatory

222 synaptic neurotransmission. Of note, the transcriptional changes were coordinated in the

223 excitatory neurons, because mostly similar time courses were observed in L5-PT, L4/5-IT, L4-IT,

224 L2/3-IT, and L5/6-IT cell types (main effect of time for *Camk1*d: P = 3 x 10^{-14}; *Grik3*: P = 0.1;

225 *Grin2b*: P = 6 x 10^{-16}; *Grin2a*: P = 1 x 10^{-14}; *Shisa9*: P = 2 x 10^{-9}; *Shisa7*: P= 5 x 10^{-10}; main

226 effect of cell type for *Camk1*d: P = 0.002; *Grik3*: P = 0.8; *Grin2b*: P = 0.1; *Grin2a*: P = 0.2;

227 *Shisa9*: P = 0.2; *Shisa7*: P= 0.2; two-way ANOVA with time and cell type as factors; **Figure 3d**).

228 Altogether, these results indicate that a main transcriptional effect of psilocybin on frontal

229 cortical excitatory neurons is to regulate synaptic function and neuronal connectivity.

230

231 **Psilocybin-induced transcriptional changes in frontal cortical GABAergic neurons**

232 **contribute to mitochondrial function and metabolic processes**

233 We next focused on GABAergic neurons and performed pseudobulk analysis on the CINs

234 (**Figure 4a**). The largest change in the number of DEGs in the CINs occurred immediately

235 following psilocybin administration, with 2222 DEGs detected at the 1-hour time point (FDR <

236 0.05; 61% upregulated and 39% downregulated; **Figure 4b**). The number of DEGs declined to 3

237 at 2 hours following administration, before climbing slowly to 8 and 8 at 4 and 24 hours and then

238 surging to 1383 at 72 hours after drug exposure (37% upregulated and 63% downregulated).

239 GO enrichment analysis revealed that DEGs in CINs were overrepresented for pathways related

240 to mitochondrial function and metabolic processes (**Figure 4c**). The engagement of these

241   pathways was strongest at the most acute 1-hour time point (main effect of time: $P = <2 \times 10^{-16}$,

242   two-sample t-test; **Supplementary Table 2**).

243

Fig. 4: Psilocybin-induced transcriptional changes in frontal cortical GABAergic neurons contribute to mitochondrial function and metabolic processes
(a) Schematic of the cortical microcircuit highlighting the PV, SST, and VIP cell types that are grouped as cortical interneurons (CINs).
(b) Differentially expressed genes (DEGs) identified by pseudobulk analysis for each time point for the CINs. Each circle represents an individual gene. Red, upregulated with FDR < 0.05. Blue, downregulated with FDR < 0.05.
(c) Top 15 terms from gene ontology enrichment analysis based on the DEGs, ranked based on the mean adjusted p-values across time points in CINs. n.p., not present. Grey, gene ontology enrichment analysis was not performed for time points with <100 DEGs with FDR < 0.05.
(d) Expression levels of specific transcripts in PV, SST, and VIP cell types following psilocybin administration, normalized to controls.

244

245   As exemplars, we plotted genes most frequently associated with the top pathways, including

246   *Cox5b*, *Cox6a1*, Cox6a2, *Eno2*, *Ndufb5*, and *Ndufs2* (**Figure 4d**). These genes had sharply

247   increased expression in CINs 1 hour following psilocybin administration (mean log$_2$(fold-change)

248   = 0.87, 0.53, 0.33, 0.72, 0.64, and 0.72, respectively) that dropped by the 2-hour timepoint

249   (mean log$_2$(fold-change) = -0.09, 0.15, 0.02, 0.03, 0.18, and 0.09, respectively). *Cox5b, Cox6a1,*

250 *and Cox6a2* encode subunits of the terminal enzyme of the mitochondrial electron transport

251 chain, cytochrome c oxidase, critical for supporting the metabolic demands of neurons through

252 oxidative phosphorylation[61]. Of note, *Cox6a2* is known to express selectively in PV interneurons

253 only to support their morphological maturation and high firing rates[62]. Disruption of *Cox6a2* has

254 been linked to mitochondrial dysfunction in the brain[63, 64]. *Eno2* encodes neuron-specific

255 enolase, a key enzyme in glycolysis and neuronal metabolism[65] with neuroprotective effects[66].

256 *Ndufb5* and *Ndufs2* encode NADH dehydrogenases that are subunits of Complex 1 in the

257 mitochondrial electron transport chain, essential for mitochondrial respiration, ATP production,

258 and oxidative stress protection[67, 68]. Transcriptional changes were largely coordinated among

259 these genes across PV, SST, and VIP cell types (main effect of time for *Cox5b*: $P = 2 \times 10^{-8}$;

260 *Cox6a1*: $P = 0.008$; *Cox6a2*: $P = 0.5$; *Eno2*: $P = 1 \times 10^{-5}$; *Ndufb5*: $P = 9 \times 10^{-4}$; *Ndufs2*: $P = 2 \times$

261 10^{-5}; main effect of cell type for *Cox5b*: $P = 0.005$; *Cox6a1*: $P = 0.1$; *Cox6a2*: $P = 0.02$; *Eno2*: P

262 $= 0.7$; *Ndufb5*: $P = 0.1$; *Ndufs2*: $P = 0.04$; two-way ANOVA with time and cell type as factors;

263 **Figure 4d**). Overall, the analyses shows that the psilocybin-induced transcriptional changes in

264 frontal cortical GABAergic neurons are involved in acutely engaging mitochondrial function and

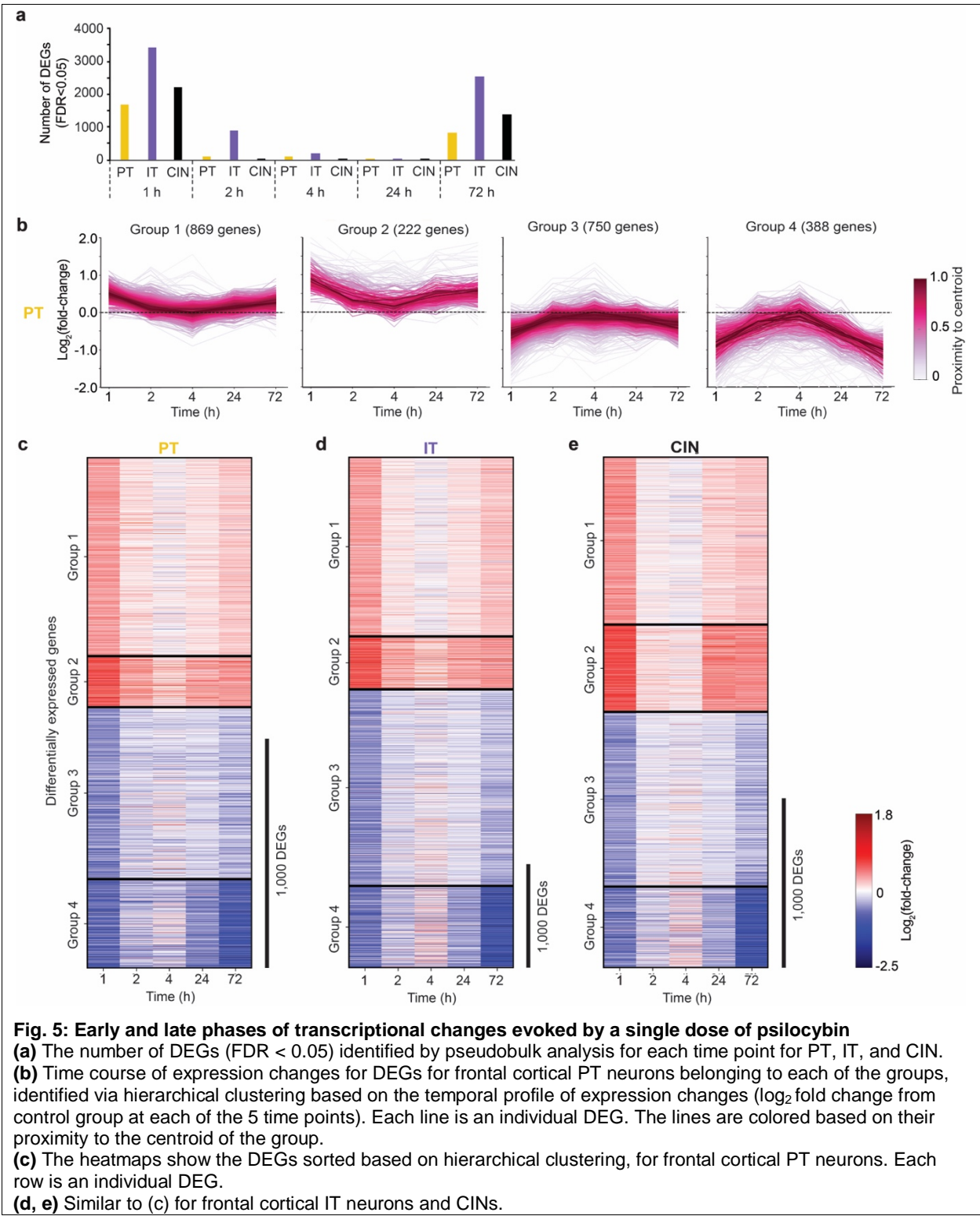265 metabolic processes.

266

267 **Early and late phases of transcriptional changes evoked by a single dose of psilocybin**

268 We next investigated the temporal dynamics in the psilocybin-induced emergence of DEGs.

269 **Figure 5a** shows the number of DEGs for the PT neurons, IT neurons, and CINs, which varied

270 significantly as a function of time (main effect of time: $P = 4.3 \times 10^{-4}$, main effect of cell group: P

271 $= 0.03$, two-factor ANOVA with time and cell type as factor)**.** The influence of psilocybin on the

272 molecular program exhibited two phases with an early response at 1 – 2 hours followed by a

273 late response detected at 72 hours after drug administration.

274

275 We surmise that the two phases of transcriptional changes could involve either the same or

276 different DEGs. To disambiguate these possibilities, we considered all DEGs in PT neurons, IT

277 neurons, and CINs, and analyzed them by performing hierarchical clustering to sort them based

278 on their temporal profile of expression changes, which revealed 4 main patterns (**Figure 5b, S3**).

279 For PT and IT neurons, most genes showed early upregulation (Group 1; PT neurons: 39% of

280 2229 DEGs, IT neurons: 35% of 4934 DEGs) or early downregulation (Group 3; PT neurons:

281 34%, IT neurons: 38%; **Figure 5c, d**). There were fewer genes that were altered during both

282 early and late phases (Group 2; PT neurons: 10%, IT neurons: 10%; Group 4; PT neurons: 17%,

283 IT neurons: 16%). Likewise, most DEGs in the GABAergic interneurons exhibited early changes

284   (33% of 3013 DEGs in Group 1 and 34% in Group 3; **Figure 5e**), rather than showing a bimodal

285   alteration across time (17% in Group 2 and 16% in Group 4). The early and late phases share

286   only a minor fraction of the DEGs, with many unique DEGs engaged only in the acute early time

287   point following psilocybin administration. GO enrichment analysis of each temporally profiled

288   group revealed differences in functional enrichment (**Figure S4**). PT neurons with early

289   upregulation (Group 1) or early downregulation (Group 3), as well as IT neurons with early

290   upregulation (Group 1) were the groups overrepresented by DEGs relating to synaptic function.

291   Meanwhile, CINs that showed upregulation during early phases (Group 1) were

292   overrepresented by DEGs relating to metabolic processes. These results provide insights into

293   the distinct phases of transcriptional responses evoked by a single dose of psilocybin.
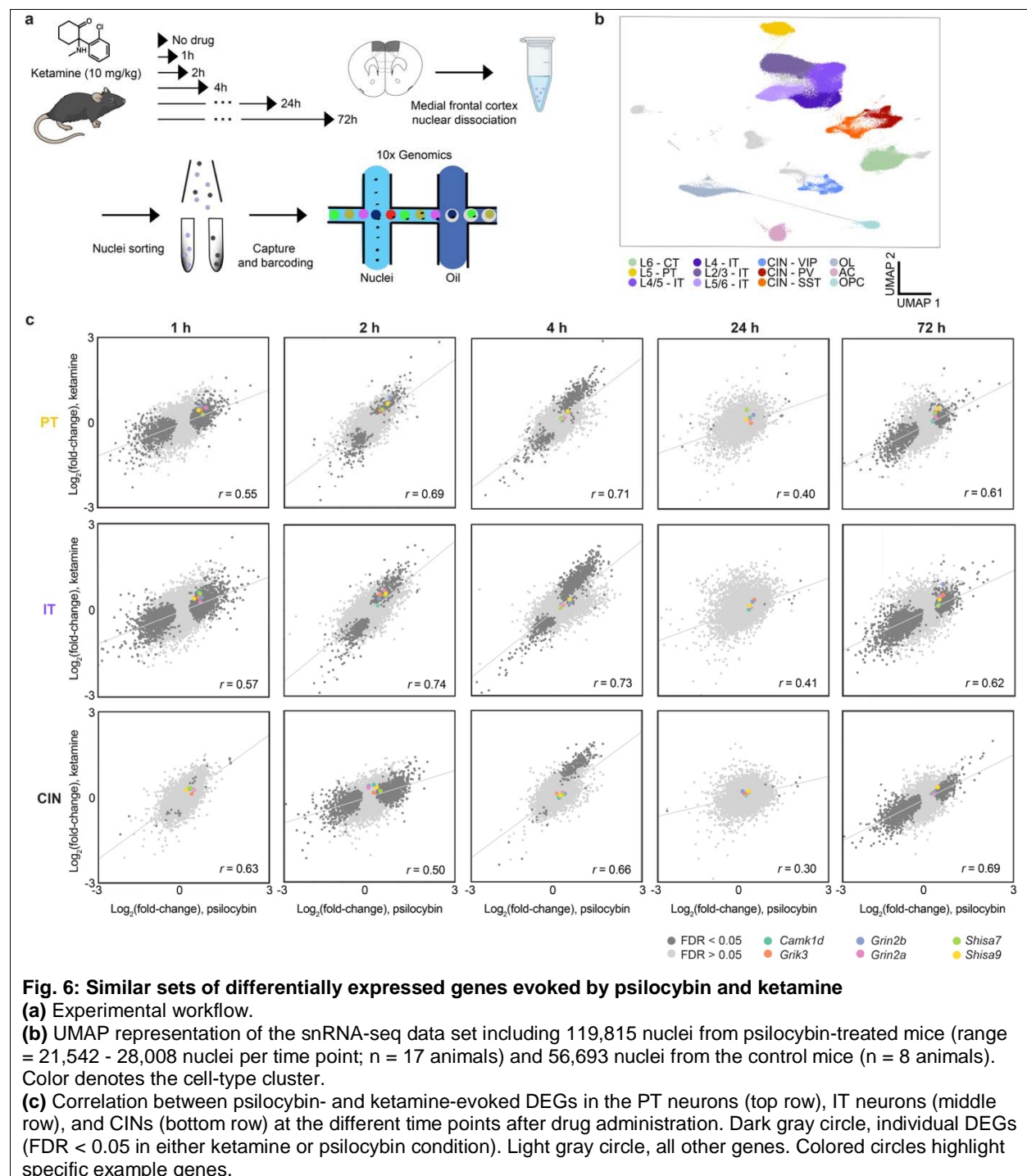
294

Fig. 5: Early and late phases of transcriptional changes evoked by a single dose of psilocybin
(a) The number of DEGs (FDR < 0.05) identified by pseudobulk analysis for each time point for PT, IT, and CIN.
(b) Time course of expression changes for DEGs for frontal cortical PT neurons belonging to each of the groups, identified via hierarchical clustering based on the temporal profile of expression changes ($\log_2$ fold change from control group at each of the 5 time points). Each line is an individual DEG. The lines are colored based on their proximity to the centroid of the group.
(c) The heatmaps show the DEGs sorted based on hierarchical clustering, for frontal cortical PT neurons. Each row is an individual DEG.
(d, e) Similar to (c) for frontal cortical IT neurons and CINs.

295

296   **Similar sets of differentially expressed genes evoked by psilocybin and ketamine**

297   Given that psilocybin is being investigated as a treatment for major depressive disorder, how do

298   these transcriptional changes in the frontal cortical cell types compare to those induced by a

299   more established rapid-acting antidepressant with a distinct molecular target? To answer this

300   question, we generated additional data from samples collected after the administration of

301   ketamine, which were obtained as part of the same experiment. Briefly, we administered

302   C57/BL6J mice with ketamine (10 mg/kg, i.p.), and dissected tissues corresponding to the

303   dorsal medial frontal cortex of both hemispheres at 1, 2, 4, 24, or 72 hours after drug

304   administration (n = 20 animals; 2 male and 2 female for each time point; **Figure 6a**). We chose

305   10 mg/kg for ketamine because this dose induces structural neural plasticity in the mouse

306   frontal cortex[69, 70, 71]. Control data were the same no-drug samples as those used for analyzing

307   the psilocybin data. The ketamine samples were processed using the same experimental

308   pipeline, yielding 139,628 cells that were sequenced at a mean depth of 8687±256 reads per

309   cell. After removing cells that did not meet quality control criteria, we had 119,815 cells from the

310   ketamine samples (range = 21,542 - 28,008 single nuclei per time point; n = 17 animals). The

311   12 cell-type clusters captured the majority of cells from ketamine-treated animals: L6-CT

312   (number of cells per time point or control condition: 3840±751), L5-PT (1418±252), L4/5-IT

313   (3643±721), L4-IT (2565±426), L2/3-IT (4290±881), L5/6-IT (2062±374), CIN-VIP (839±136),

314   CIN-PV (1379±240), CIN-SST (1003±156), oligodendrocytes (2386±547), astrocytes

315   (1530±308), and OPCs (1105±218) (**Figure 6b**, **Supplementary Table 1**). The same cell-type

316   clusters were detected across samples collected at different time points after ketamine

317   administration (**Figure S5**). We identified differentially expressed genes in PT neurons, IT

318   neurons, and CINs at different times points after the single dose of ketamine (**Figure S6, S7, S8,**

319   **S9**).

320

Fig. 6: Similar sets of differentially expressed genes evoked by psilocybin and ketamine
(a) Experimental workflow.
(b) UMAP representation of the snRNA-seq data set including 119,815 nuclei from psilocybin-treated mice (range = 21,542 - 28,008 nuclei per time point; n = 17 animals) and 56,693 nuclei from the control mice (n = 8 animals). Color denotes the cell-type cluster.
(c) Correlation between psilocybin- and ketamine-evoked DEGs in the PT neurons (top row), IT neurons (middle row), and CINs (bottom row) at the different time points after drug administration. Dark gray circle, individual DEGs (FDR < 0.05 in either ketamine or psilocybin condition). Light gray circle, all other genes. Colored circles highlight specific example genes.

321

322　　To compare the transcriptional changes evoked by psilocybin and ketamine, we generated

323　　scatter plots to correlate the drug-evoked expression changes in all genes. This analysis

324　　revealed a highly significant positive correlation in the psilocybin- and ketamine-evoked sets of

325　　altered genes in PT neurons, IT neurons, and CINs (all with $r >= 0.6$; **Figure 6c**). Essentially,

326　　genes that were upregulated by psilocybin tended to be also upregulated by ketamine, whereas

327   genes that were downregulated by psilocybin were similarly downregulated by ketamine. These

328   results show similar transcriptional changes in the mouse medial frontal cortex evoked by a

329   single dose of ketamine or psilocybin.

330

331   **DISCUSSION**

332   The present study applied single-nucleus transcriptomics to determine how the classic

333   psychedelic psilocybin alters gene expression in the mouse medial frontal cortex. There are

334   three main findings. One, excitatory and GABAergic neurons exhibit distinct sets of differentially

335   expressed genes with roles in regulating synaptic plasticity and controlling metabolic processes

336   respectively. Two, psilocybin's impact is time-dependent with early and late phases of

337   transcriptional responses. Three, psilocybin and ketamine evoke highly similar patterns of gene

338   expression changes. Our results therefore unveil the dynamics and diversity of transcriptional

339   responses in frontal cortical cell types after a single dose of psilocybin.

340

341   Analyses of our snRNA-seq data set and the Allen Institute's database show that most

342   excitatory and GABAergic neurons express serotonin receptor subtypes and are thus likely

343   direct targets of classic psychedelics. The psilocybin-evoked transcriptional changes in

344   excitatory neurons indicate a coordinated response across PT and IT cell types on synaptic

345   plasticity pathways. This spotlight on regulation of synaptic function is consistent with the

346   numerous reports of psychedelic-induced structural neural remodeling in cortical pyramidal

347   neurons[7, 8, 37, 72, 73]. In GABAergic neurons, we found that psilocybin-induced transcriptional

348   changes were dominated by pathways related to mitochondrial and metabolic processes.

349   This may be a direct effect, because 5-HT$_{2A}$ receptor activation can influence mitochondrial

350   biogenesis and function in cortical neurons by engaging the SIRT1-PGC-1α axis[74]. Psilocybin

351   may engage similar mechanisms to regulate cellular metabolism in CINs. Alternatively, this may

352   be an indirect consequence due to drug-evoked spiking activity in GABAergic neurons, as that

353   would likely trigger an acute upregulation of oxidative stress protection, especially to support the

354   high-energy repetitive firing in PV interneurons[62].

355

356   The bolus injection of psilocybin causes rapid elevation of drug concentration in the central

357   nervous system followed by full clearance within a few hours. The pharmacokinetics hints at a

358   time course of transcriptional changes, and here we uncovered an early phase at 1 – 2 hours

359   followed by a late phase at 72 hours with high numbers of differentially expressed genes. Our

360   findings echo the framework that there are often multiple waves of transcription following a

361 perturbation[10, 75]. For example, there are early and late response genes in visual cortical cells in

362 dark-reared animals after their first experience of visual stimuli[76]. The timing of the activity-

363 dependent transcription varies depending on the neuronal spiking pattern[77], suggesting that

364 different phases of transcriptional responses may relate to psilocybin's distinct effects on the

365 firing of different frontal cortical cell types. Furthermore, a previous study suggested that the

366 early and sustained antidepressant effects of ketamine may depend on distinct neural

367 mechanisms[71]. It is tempting to speculate that the multiple phases of transcriptional responses

368 observed in this study may reflect therapeutic mechanisms at different time scales.

369

370 There are limitations for this study. Transcriptomics is a rapidly growing field with numerous

371 approaches for sequencing and analysis. Here, we chose to work with single nuclei instead of

372 single cells, because we were concerned that cortical neurons with extended axons and

373 dendrites may be damaged in protocols needed to dissociate single cells, which can lead to

374 aberrant readout of gene expression[78, 79]. Sequencing with single nuclei may better reflect

375 recent changes in *de novo* transcription, and has been shown to yield excellent sensitivity and

376 reliable classification of cell types[80]. Our results should be readily comparable to the increasing

377 number of snRNA-seq data sets, including those collected from individuals with major

378 depression[81, 82] or substance use phenotypes[83], and from animal models following exposure to

379 drugs such as cocaine[21, 22] and DOI[14]. A caveat is that we compared the effects of psilocybin at

380 different time points against controls that were acquired at the "zero time point", without drug

381 administration. An ideal control would be vehicle-injected animals collected at the same 5 time

382 points, but we were constrained by the costs associated with sequencing. Anticipating the

383 importance of having high-quality data from controls for our analysis, we increased the size of

384 the drug-free samples to 9 animals instead of the 4 animals used for each time point for each

385 drug condition.

386

387 Like psilocybin, ketamine is a compound that elicits acute psychological changes followed by

388 longer-term antidepressant effects. Ketamine is primarily a NMDA receptor antagonist. Although

389 psilocybin and ketamine have distinct molecular targets, they seemingly converge to produce

390 similar effects on neural structural plasticity and behavior. In this study, a head-to-head

391 comparison between psilocybin and ketamine reveals striking parallels in the transcriptional

392 responses at the medial frontal cortex, suggesting shared molecular mechanisms that may

393 underpin their behavioral effects. The overlapping patterns of transcriptional regulation raise an

394 intriguing possibility of a transcriptional fingerprint that may be unique to rapid-acting

395   antidepressants. We anticipate the growing number of studies revealing the molecular and

396   cellular impact of psilocybin and ketamine will eventually reveal mechanisms of action that can

397   accelerate the development of more effective and safer drugs for treating mental illnesses.

398

399   **METHODS**

400

401   **Animals.** Animal care and experimental procedures were approved by the Animal Care & Use

402   Committee (IACUC) at Yale University. C57BL/6J (Stock No. 000664) mice were purchased

403   from Jackson Laboratory and habituated in our animal facility at Yale University for 1 week.

404   Animals were housed in same-sex groups of 2-5 mice per cage in a temperature-controlled

405   room, operating in normal 12 hr light - 12 hr dark cycle (8:00 AM to 8:00 PM for light). Food and

406   water were available ad libitum. Animals were randomly assigned to different experimental

407   groups. 20 mice (10 males and 10 females) were assigned to the psilocybin-treated group and

408   20 mice (10 males and 10 females) were assigned to the ketamine-treated group. 8-week-old

409   animals were injected with psilocybin (1 mg/kg, i.p, prepared from working solution, which was

410   made fresh monthly from powder; Usona Institute) or ketamine (10 mg/kg, i.p; Zoetis), returned

411   to their home cage, and used 1, 2, 4, 24, or 72 hours after injection. 9 mice (3 males and 6

412   females) were used with no drug administration as controls.

413

414   **Tissue collection and generation of single-cell suspensions.**

415   For tissue collection, decapitation immediately followed cervical dislocation and brains were

416   immediately dissected from the skull. The dorsal medial frontal cortex, consisting of ACAd and

417   medial MOs, was microdissected in cold RNAse-free 1x PBS, flash frozen in ethanol and dry

418   ice, and stored at -80°C. Samples were shipped overnight on dry ice to the University of

419   Michigan for processing. Nuclei were isolated and processed for single-nucleus sequencing

420   using RNase-free materials and reagents. Fresh buffers were made immediately before nuclei

421   processing. Buffers were made in accordance with recommended protocol (CG000393 Rev A,

422   "Nuclei isolation from adult mouse brain tissue for single cell RNA sequencing", 10x Genomics).

423   Lysis buffer consisted of 10 mM Tris-HCl ph7.4 (Millipore-Sigma T2194), 10 mM NaCl (Millipore-

424   Sigma 59222C), 3 mM $MgCl_2$ (Millipore-Sigma, M1028), 0.1% Nonidet P40 (Millipore-Sigma

425   74385), and nuclease-free water (Invitrogen AM9932). Wash buffer consisted of 1% BSA

426   solution (Thermo Fisher Scientific AM2616), 0.2U/μl RNase Inhibitor (Millipore-Sigma

427   3335399001), and 1x PBS (Gibco, 10010023). Tissue was dounce homogenized in 1 mL lysis

428   buffer and centrifuged at 500g for 5 minutes at 4°C. Supernatant was removed and samples

429   were resuspended in 1mL of wash buffer. Samples were strained through 40 μm cell strainers

430   (Bel-Art H13680-0040) and centrifuged again at 500 g for 5 minutes at 4°C. Supernatant was

431   removed and samples were resuspended in 1mL of wash buffer and passed through 40 μm cell

432   strainers once more. Nuclei were visually checked with Trypan Blue Stain (Thermo Fisher

433   Scientific T10282) to ensure minimal debris and efficient lysis. Nuclei were stained with 0.25 μL

434   7AAD (Invitrogen A310) and immediately flow sorted and counted on a MoFlo Astrios (Beckman

435   Coulter) at the North Campus Research Complex Flow Core at University of Michigan to reduce

436   ambient RNA. Samples were centrifuged and resuspended in wash buffer at a concentration of

437   1,000 cells/μL.

438

439   **Single cell library preparation and sequencing.** Library prep and next-generation sequencing

440   were carried out in the Advanced Genomics Core at the University of Michigan. Resulting

441   libraries were sequenced on the Illumina NovaSeq S4 300 cycle, at a target depth of 25,000

442   reads/cell and a target of 10,000 cells/sample.

443

444   **Single cell quality control, clustering, and cell type identification.** Single nucleus RNA

445   sequencing at the University of Michigan Advanced Genomics Core returned demultiplexed

446   FASTQ files from all 49 samples. The 10x Genomics Mouse mm10 (GENCODE

447   vM23/Ensembl98) reference version 2020-A was downloaded as a reference genome. FASTQ

448   files were processed with 10x Genomics cellranger count version 7.1.0 and aligned to this

449   reference, including intronic reads.

450

451   Preprocessing and further analysis relied on anndata[84] (version 0.8.0) and scanpy[85] (version

452   1.10.3). Filtered feature-barcode matrices for all samples and all drug treatments were imported

453   to AnnData objects and concatenated using anndata.concat() on the intersection of genes. One

454   sample was not included in the study due to low cell numbers, 4 were excluded for

455   oversequencing, and 2 were dropped for large batch effects. A total of 42 samples that met all

456   quality control measures were further processed. All genes detected in fewer than 3 unique

457   nuclei or having fewer than 5 total transcript counts were removed. All nuclei with fewer than 3

458   unique genes detected or having fewer than 5 total transcript counts were removed. Multiplet

459   nuclei were identified and removed with scanpy.pp.scrublet() including a batch key identifying

460   individual samples[86]. Nuclei with low transcript counts on a per-sample basis (<1000 counts and

461   less than 3 mean absolute deviations below the median) were removed. Cells with high

462   mitochondrial or ribosomal counts on a per-sample basis (>20% of counts or more than 3 mean

463   absolute deviations above the median) were removed. Ribosomal genes based on the

464   Ribosomal Protein Gene Database[87] (http://ribosome.med.miyazaki-u.ac.jp/) were removed

465   from analysis. The ubiquitously overexpressed *Malat1* gene was removed from analysis.

466

467   All nuclei libraries were randomly downsampled without replacement to 1000 transcripts with

468   scanpy.pp.downsample_counts(), and nuclei with less than 1000 transcripts were removed.

469   Each cell's reads were normalized to counts per million (CPM) with scanpy.pp.normalize_total(),

470   and a natural logarithm was taken with scanpy.pp.log1p()[88]. This yielded ln(CPM+1), which was

471   used for all downstream expression analysis except pseudobulk. We selected the top 5000

472   highly variable genes using scanpy.pp.highly_variable_genes() with flavor='seurat' and these

473   were used to compute the top 236 principal components, which encompassed 50% of the

474   overall variation in the highly variable genes. The nearest neighbors graph was constructed with

475   scanpy's batch corrected K nearest neighbors algorithm scanpy.pp.bbknn(). This was input to

476   Uniform Manifold Approximation Projection[89] (UMAP) and Leiden clustering with resolution 1.0.

477   Cell types were hand-annotated based on the marker gene results from

478   scanpy.tl.rank_genes_groups() with the Wilcoxon rank-sum test. Cell type identification was

479   based on marker gene expression congruence with earlier work[90]. Example marker genes for

480   L2/3-IT: *Rasgrf2*, *Calb1*; L6-CT: *Foxp2*, *Hs3st4*; L4/5-IT: *Il1rapl2*; L4-IT: *Rorb*; L5/6-IT: *Galnt14*,

481   *Sulf1*; L5-PT: *Coro6*, *Parm1*; CIN-PV: *Pvalb*; CIN-SST: *Sst*; CIN-VIP: *Vip*; oligodendrocytes:

482   *Mbp*, *Plp1*; astrocytes: *Slc1a2*, *Clu*; OPC: *Olig2*.

483

484   **Cell-type specific analysis.** We performed more in-depth analysis on the response relationship

485   of the following cell types: excitatory neurons (L2/3-IT, L6-CT, L4/5-IT, L4-IT, L5/6-IT, L5-PT),

486   cortical interneurons (CIN-PV, CIN-SST, CIN-VIP), and glial cells (oligodendrocytes, astrocytes,

487   OPC). We use hierarchical clustering to classify these cell types based on transcriptional

488   profiles over all cells with scanpy.tl.dendrogram() and we recomputed the top marker genes

489   based on these cell types only with scanpy.tl.rank_genes_groups(). We plotted the expression

490   of the top 3 marker genes for each cell type with scanpy.pl.heatmap().

491

492   **5-HT receptor expression.** To examine cell-type specific expression patterns of psilocybin's

493   main 5-HT receptor targets, we extracted *Htr1a*, *Htr2a*, and *Htr2c* transcript levels from the

494   control samples in our snRNA-seq data set (i.e., control samples from no-drug condition). Cell

495   type-specific patterns were visualized on a per-cell basis on the data set's UMAP

496   representation. Group-wise variation among distinct cell subtypes (see below) was visualized

497   with violin plots. UMAPs were created using matplotlib and the scanpy UMAP embeddings of

498   the dataset, while violin plots were constructed using scanpy.pl.violin(). The scale of expression

499   was unified across all genes by identifying the maximum expression level.

500

501   Transcript levels from our snRNA-seq dataset were compared to publicly available single-cell

502   sequencing data set from the Allen Institute for Brain Science (https://portal.brain-

503   map.org/atlases-and-data/rnaseq/mouse-whole-cortex-and-hippocampus-smart-seq). Briefly,

504   this independent dataset used SMARTseq-v4 to analyze 76,381 single cell transcriptomes

505   across the mouse cortex and hippocampus, and cluster these cells into transcriptional cell

506   subtypes[46, 91]. We selected the 17,461 cells sampled in frontal cortex regions (ACA, ALM, ORB,

507   and PL-ILA), including 84 micro_PVM, 118 oligo, 277 astro, 1403 L2/3 IT, 3118 L4/5 IT, 1541 L5

508   IT, 640 L6 IT, 471 L5 PT, 2159 L6 CT, 1009 L5/6 NP, 579 L6b, 1174 Pvalb, 382 Sncg, 1708

509   Vip, 126 Sst Chodl, 1573 Sst, and 1099 Lamp5 as identified and annotated already by the Allen

510   Institute. Transcript levels for 5-HT receptors (*Htr1a*, *Htr1b*, *Htr1d*, *Htr2a*, *Htr2b*, *Htr2c*, *Htr3a*,

511   *Htr3b*, *Htr4*, *Htr5a*, *Htr5b*, *Htr6*, *Htr7*), as well as cell type markers for excitatory (*Slc17a7*) or

512   inhibitory (*Gad1*, *Pvalb*, *Cck*, *Vip*, *Sst*, *Ndnf*) neurons were extracted for each cell subtype.

513   Expression levels were depicted in a dot plot showing $\log_2(CPM+1)$ per cell type, with dot size

514   scaled by the percentage of cells of that type with non-zero transcript reads. Processing and

515   visualization of Allen Institute data were done using MATLAB scripts.

516

517   **Differential gene expression using pseudobulk.** We performed primary cell-type specific

518   differential expression analysis using pseudobulk techniques to identify genes of interest while

519   minimizing the risk of false discoveries. For pseudobulk, raw un-normalized transcript counts

520   were sum aggregated within cell types[92] or within a group of cell types when appropriate.

521   Differential expression testing was performed with edgeR[53]. Genes with less than 10 total

522   counts were excluded using edgerR::filterByExpr(). Differential expression was measured with

523    $\log_2$(fold-change) and p-values were adjusted false discovery rate (FDR) correction. Genes

524   were identified as significant with an FDR below 5%. ggplot2 and kwanlibr were used to create

525   volcano plots. Genes with $\log_2$(fold-change) or $-\log_{10}$(p-value) beyond the bounds of the plot

526   area were clamped to be displayed on the axis limits. We used two-side hypothesis test on

527    $H_0: log_2\ FC\ =\ 0$ and corrected p-values with false discovery rate correction. We used an FDR

528   threshold of 0.05 to identify significantly differentially expressed genes.

529

530 **DEG similarity between cell types using memento.** We conducted an additional cell-type

531 specific differential expression analysis of control vs drug-treated cells using an alternative

532 independent tool: Memento[52]. Memento uses an efficient bootstrapping method alongside

533 method of moments estimation to compare the distributional parameters of genes' differential

534 expression, while making no assumptions about the underlying transcript count distribution.

535 Memento analysis estimated both drug dependent and time dependent changes by using sex as

536 a covariate and time after treatment as a factor of interest. Sequencing saturation was taken

537 from the cellranger count 10x_metrics.csv output and multiplied by 0.25 to obtain the capture

538 rate, as instructed by memento documentation. We used the memento ht_1d_moments function

539 with 5000 bootstraps. Differential expression was measured with log2 fold change and p-values

540 were adjusted False Discovery Rate correction. We used two-side hypothesis test on

541 $H_0: log_2 FC = 0$. We used an FDR threshold of 0.05 to identify significantly differentially

542 expressed genes. We generated heatmaps to show the similarity in differential expression

543 between cell types within a certain drug treatment and time after treatment. For each pair of cell

544 types, we retrieved their memento differential expression results compared to control from the

545 corresponding timepoint. For each cell type, we found the 1000 differentially expressed genes

546 with the most significant FDR. We computed cosine similarity on the log_2(fold-change) of these

547 vectors, filling in missing values from the join with zeros for compatibility between the vectors.

548 We performed this analysis at each treatment time point (1, 2, 4, 24, and 72 h) and for each

549 drug (psilocybin, ketamine).

550

551 **Grouping of cell types for downstream analysis.** To support our choice to group IT neurons

552 together, CIN neurons together, and analyze other cell types individually, we assessed many

553 potential clustering of cell types. The Calinski-Harabasz index measures how tightly members

554 within the same cluster are grouped compared to how spread out different clusters are. Higher

555 values indicate better clustering. This metric utilizes within-cluster sum of squares (WCSS) and

556 between-cluster sum of squares (BCSS). We computed the relative cosine distances between

557 cell types based on the cosine similarity of their differential expression under psilocybin

558 compared to control cells. However, both BCSS and WCSS rely on absolute embeddings of

559 individual items. We therefore use mCHI, a modified Calinski Harabasz index here. When we

560 define a cluster of cell types, the cluster does not have a centroid for the above reason.

561 Therefore, instead of computing the BCSS, which measures the sum-squared distances from

562 cluster centroids to the data centroid, we compute a modified BCSS (mBCSS). For any pair of

563 clusters A and B, we define the distance between them as the average distance between their

564 bipartite members. mBCSS is the square of this average distance, summed over all pairs of

565 clusters. Let C be the clustering. Let P_C be the set of all combinatorial pairs (a,b) of clusters of

566 the clustering C. Let d(i,j) be the cosine distance between 2 cell types summed across all 5

567 treatment timepoints. Then

$$mBCSS(C) = \sum_{(a,b) \in P_C} \left(\frac{1}{|a||b|} \sum_{i \in a, j \in b} d(i,j) \right)^2$$

568

569 Similarly, we cannot compute the distance between a cluster member and its centroid as WCSS

570 requires, so instead we compute modified WCSS (mWCSS). mWCSS is the sum of the squared

571 distance between two cell types, for all pairs of cell types in the same cluster and for all clusters.

572 Let C be the clustering. Let P_a be the set of all combinatorial pairs (i,j) of cell types in cluster a.

573 Let d(i,j) be the cosine distance between 2 cell types summed across all 5 treatment timepoints.

574 Then

$$mWCSS(C) = \sum_{a \in C} \sum_{(i,j) \in P_a} d(i,j)^2$$

575

576 In computing the modified Calinsky-Harabasz index, we directly replace BCSS and WCSS with

577 mBCSS and mWCSS respectively, and maintain the standard degrees of freedom. Then for a

578 clustering C,

$$mCHI(C) = \frac{mBCSS(C)/(k-1)}{mWCSS/(n-k)}$$

579

580 For the clustering of [L6-CT, L5-PT, L4/5-IT, L4-IT, L2/3-IT, L5/6-IT] and [CIN-VIP, CIN-PV, CIN-

581 SST], mCHI is 0.127. For the clustering of [L5-PT], [L6-CT, L4/5-IT, L4-IT, L2/3-IT, L5/6-IT],

582 [CIN-VIP, CIN-PV, CIN-SST], mCHI is 0.203. For the clustering of [L6-CT], [L5-PT], [L4/5-IT, L4-

583 IT, L2/3-IT, L5/6-IT], [CIN-VIP, CIN-PV, CIN-SST], mCHI is 0.278.

584

585 **Temporal profiles of DEGs.** To identify genes responsible for the early and late waves of

586 differential expression under psilocybin, we clustered differentially expressed genes based on

587 their temporal expression profile. Due to our interest in specific genes, data for this analysis

588 came from pseudobulk differential expression to minimize the risk of false discoveries. For each

589 of PT, IT, and CIN, we identified genes that were significantly differentially expressed at any

590 time point and retrieved their profile of differentially expressed $\log_2$(fold-change) across each

591   time point, yielding a vector. We accumulated this list across the 3 cell types, maintaining

592   multiple profiles if a single gene was differentially expressed in multiple cell types. This yielded

593   10,176 unique differentially expressed profiles.

594

595   We used hierarchical clustering, specifically bisecting K-means from sklearn to cluster the

596   genes by their temporal profiles. We tested between 2 and 20 clusters to tune for the optimal

597   number of clusters. Inertia, or within-cluster sum of squares, continuously decreases as

598   expected as we increase the number of clusters, but the incremental drops in inertia from

599   adding one more cluster becomes smaller as the number of clusters increases. This drop in

600   efficiency led us to prioritize fewer clusters. Additionally, we saw that after 4 clusters, adding any

601   additional clusters did not yield any new distinctive temporal profile shapes, or that new

602   temporal profiles shared significant overlap with already existing clusters. Furthermore, adding

603   additional clusters seemed to only split up already small clusters instead of dominant clusters,

604   which means outlier genes were driving the clustering at higher numbers of clusters. This led us

605   to choose 4 clusters for our analysis. After grouping genes into one of 4 clusters with bisecting

606   K-means, we computed the Euclidean distance of each gene g to its cluster centroid, d(g). We

607   also defined centroid proximity as how close a gene is to its centroid, inversely to distance, as

608   prox(g) = exp(-2 d(g)). Since distance is strictly positive real numbers, this proximity metric

609   yields values where smaller distances to centroid have proximity close to 1, while farther

610   distances to centroid have proximity close to 0. Taking the square yields a symmetric

611   distribution of proximity. This distribution was plotted for each cell type using seaborn.kdeplot()

612   with default bandwidth and without common normalization. Line plots of genes for each

613   temporal profile group were generated independently for each cell type. Darker lines have

614   higher proximity to centroid, while lighter lines have lower proximity. Additionally, we plotted the

615   mean differential expression of genes in each group. The width of the error band was computed

616   using the 95th percentile interval over all genes within the group using seaborn. Heatmaps show

617   the expression progression profiles of these genes. Red represents positive $\log_2$(fold-change),

618   blue represents negative $\log_2$(fold-change), and white represents no change. Each row in the

619   heatmap represents a gene.

620

621   **Comparison of differential expression between psilocybin and ketamine.** To compare the

622   transcriptional reaction of genes between psilocybin and ketamine treatment, we directly

623   compared differential expression of psilocybin cells to ketamine cells from the pseudobulk

624   analysis. For each time point and the 3 major cell types we analyzed, we made a scatter plot of

625    $\log_2$(fold-change) response to psilocybin on the x-axis and $\log_2$(fold-change) response to

626   ketamine on the y-axis. Genes that were significantly differentially expressed (FDR < 0.05) in

627   either psilocybin or ketamine drug treatment were colored dark grey, and some genes of interest

628   were highlighted. We computed and plotted the linear regression of ketamine $\log_2$(fold-change)

629   and psilocybin $\log_2$(fold-change) using scipy.stats.linregress() using all genes. Similarly, we also

630   computed the Pearson correlation coefficient using all genes with scipy.stats.pearsonr().

631

632   **Gene ontology analysis.** Gene ontology (GO) analysis was performed using Enrichr[93, 94, 95]

633   and Gene Ontology Biological Processes 2023 database to identify biological processes that

634   were overrepresented for genes that were differentially expressed. For each time point with a

635   minimum of 100 DEGs (FDR < 0.05), the DEGs were analyzed using Enrichr. The adjusted p-

636   values were computed by Enrichr using the Benjamini-Hochberg procedure for multiple

637   hypotheses testing correction. To select the top GO terms for excitatory cells, we considered PT

638   and IT neurons together, averaging the $-\log_{10}$(adjusted p-value) from GO analysis across PT

639   and IT neurons and across time points to rank the GO terms. We only included GO terms that

640   were present from GO analysis for at least two time points. To select the top GO terms for

641   cortical interneurons, we averaged adjusted $-\log_{10}$(adjusted p-value) from GO analysis across

642   timepoints to rank the GO terms. For statistical analysis, we performed ANOVA using the

643   adjusted p-values. If a term was not present at a certain time point, the value was imputed to 1

644   for the purpose of the statistical analysis. To identify representative genes, we first determined

645   the 3 most frequent associated genes for each of the top 30 GO terms across all time points.

646   From this refined list, we then hand-selected genes of interest.

647

648   **DATA AVAILABILITY**

649   Raw sequencing data associated with this study have been submitted to the NIH Sequence

650   Read Archive under BioProject ID PRJNA1204073

651   (http://www.ncbi.nlm.nih.gov/bioproject/1204073).

652

653   **CODE AVAILABILITY**

654   Computer code to process and analyze the snRNA-seq data is provided as Snakemake scripts,

655   Jupyter notebooks, and R scripts on GitHub

656   (https://github.com/thekwanlab/psilocybin_cortex_snRNAseq).

657

ACKNOWLEDGEMENTS

CONTRIBUTIONS

C.L, K.Y.K., and A.C.K planned the study. C.L. conducted the experiment. E.O. and Y.Q. performed the analysis. C.L. assisted in the analysis. N.K.S. and A.C.K. analyzed the data from Allen Institute. M.J.G. contributed to the planning of the study. C.L., K.Y.K., and A.C.K. drafted the manuscript. All authors reviewed the manuscript before submission.

DISCLOSURES

A.C.K. has been a scientific advisor or consultant for Boehringer Ingelheim, Empyrean Neuroscience, Freedom Biosciences, and Psylo. A.C.K. has received research support from Intra-Cellular Therapies. The other authors report no financial relationships with commercial interests.

SUPPLEMENTAL TABLES

Table S1. The number of cells in each experimental group.

Table S2. Statistical analyses associated with Figure 3c, 3d, 4c, 4d, and 5a.

Table S3. Details for gene ontology (GO) enrichment analyses including pathway and ID.

REFERENCES

1.	Goodwin GM*, et al.* Single-Dose Psilocybin for a Treatment-Resistant Episode of Major Depression. *N Engl J Med* **387**, 1637-1648 (2022).

2.	Davis AK*, et al.* Effects of Psilocybin-Assisted Therapy on Major Depressive Disorder: A Randomized Clinical Trial. *JAMA Psychiatry* **78**, 481-489 (2021).

3. Carhart-Harris R, *et al.* Trial of Psilocybin versus Escitalopram for Depression. *N Engl J Med* **384**, 1402-1411 (2021).

4. Raison CL, *et al.* Single-Dose Psilocybin Treatment for Major Depressive Disorder: A Randomized Clinical Trial. *JAMA* **330**, 843-853 (2023).

5. von Rotz R, *et al.* Single-dose psilocybin-assisted therapy in major depressive disorder: A placebo-controlled, double-blind, randomised clinical trial. *EClinicalMedicine* **56**, 101809 (2023).

6. Liao C, Dua AN, Wojtasiewicz C, Liston C, Kwan AC. Structural neural plasticity evoked by rapid-acting antidepressant interventions. *Nat Rev Neurosci*, in press (2024).

7. Ly C, *et al.* Psychedelics Promote Structural and Functional Neural Plasticity. *Cell Rep* **23**, 3170-3182 (2018).

8. Shao LX, *et al.* Psilocybin induces rapid and persistent growth of dendritic spines in frontal cortex in vivo. *Neuron* **109**, 2535-2544 e2534 (2021).

9. Shao LX, *et al.* Pyramidal cell types and 5-HT2A receptors are essential for psilocybin's lasting drug action. *biorxiv*, (2024).

10. Yap EL, Greenberg ME. Activity-Regulated Transcription: Bridging the Gap between Neural Activity and Behavior. *Neuron* **100**, 330-348 (2018).

11. Ma H, *et al.* Excitation–transcription coupling, neuronal gene expression and synaptic plasticity. *Nature Reviews Neuroscience* **24**, 672-692 (2023).

12. Gonzalez-Maeso J, *et al.* Transcriptome fingerprints distinguish hallucinogenic and nonhallucinogenic 5-hydroxytryptamine 2A receptor agonist effects in mouse somatosensory cortex. *J Neurosci* **23**, 8836-8843 (2003).

13. Desouza LA, *et al.* The Hallucinogenic Serotonin2A Receptor Agonist, 2,5-Dimethoxy-4-Iodoamphetamine, Promotes cAMP Response Element Binding Protein-Dependent Gene Expression of Specific Plasticity-Associated Genes in the Rodent Neocortex. *Front Mol Neurosci* **14**, 790213 (2021).

14. Muir J, *et al.* Isolation of psychedelic-responsive neurons underlying anxiolytic behavioral states. *Science* **386**, 802-810 (2024).

15. Gonzalez-Maeso J, *et al.* Hallucinogens recruit specific cortical 5-HT(2A) receptor-mediated signaling pathways to affect behavior. *Neuron* **53**, 439-452 (2007).

16. Nichols CD, Sanders-Bush E. A single dose of lysergic acid diethylamide influences gene expression patterns within the mammalian brain. *Neuropsychopharmacology* **26**, 634-642 (2002).

17. Nogueira M, *et al.* Serotonergic psychedelic 5-MeO-DMT alters plasticity-related gene expression and generates anxiolytic effects in stressed mice. *Mol Psychiatry*, (2024).

18. Jefsen OH, Elfving B, Wegener G, Muller HK. Transcriptional regulation in the rat prefrontal cortex and hippocampus after a single administration of psilocybin. *J Psychopharmacol* **35**, 483-493 (2021).

19. Donovan LL*, et al.* Effects of a single dose of psilocybin on behaviour, brain 5-HT2A receptor occupancy and gene expression in the pig. *Eur Neuropsychopharmacol* **42**, 1-11 (2021).

20. Walker DM*, et al.* Cocaine Self-administration Alters Transcriptome-wide Responses in the Brain's Reward Circuitry. *Biol Psychiatry* **84**, 867-880 (2018).

21. Savell KE*, et al.* A dopamine-induced gene expression signature regulates neuronal function and cocaine response. *Sci Adv* **6**, eaba4221 (2020).

22. Phillips RA, 3rd*, et al.* Distinct subpopulations of D1 medium spiny neurons exhibit unique transcriptional responsiveness to cocaine. *Mol Cell Neurosci* **125**, 103849 (2023).

23. Browne CJ*, et al.* Transcriptional signatures of heroin intake and relapse throughout the brain reward circuitry in male mice. *Sci Adv* **9**, eadg8558 (2023).

24. Engeln M*, et al.* Transcriptome profiling of the ventral pallidum reveals a role for pallido-thalamic neurons in cocaine reward. *Mol Psychiatry* **27**, 3980-3991 (2022).

25. Nardou R*, et al.* Psychedelics reopen the social reward learning critical period. *Nature* **618**, 790-798 (2023).

26. Bagot RC*, et al.* Ketamine and Imipramine Reverse Transcriptional Signatures of Susceptibility and Induce Resilience-Specific Gene Expression Profiles. *Biol Psychiatry* **81**, 285-295 (2017).

27. Walker DM*, et al.* Sex-Specific Transcriptional Changes in Response to Adolescent Social Stress in the Brain's Reward Circuitry. *Biol Psychiatry* **91**, 118-128 (2022).

28. Bagot RC*, et al.* Circuit-wide Transcriptional Profiling Reveals Brain Region-Specific Gene Networks Regulating Depression Susceptibility. *Neuron* **90**, 969-983 (2016).

29. Pena CJ*, et al.* Early life stress confers lifelong stress susceptibility in mice via ventral tegmental area OTX2. *Science* **356**, 1185-1188 (2017).

30. Pena CJ*, et al.* Early life stress alters transcriptomic patterning across reward circuitry in male and female mice. *Nat Commun* **10**, 5098 (2019).

31. Vollenweider FX, Vollenweider-Scherpenhuyzen MF, Babler A, Vogel H, Hell D. Psilocybin induces schizophrenia-like psychosis in humans via a serotonin-2 agonist action. *Neuroreport* **9**, 3897-3902 (1998).

32. Madsen MK*, et al.* Psychedelic effects of psilocybin correlate with serotonin 2A receptor occupancy and plasma psilocin levels. *Neuropsychopharmacology* **44**, 1328-1334 (2019).

33. Hasler F, Bourquin D, Brenneisen R, Bar T, Vollenweider FX. Determination of psilocin and 4-hydroxyindole-3-acetic acid in plasma by HPLC-ECD and pharmacokinetic profiles of oral and intravenous psilocybin in man. *Pharm Acta Helv* **72**, 175-184 (1997).

34. Preller KH*, et al.* Psilocybin Induces Time-Dependent Changes in Global Functional Connectivity. *Biol Psychiatry* **88**, 197-207 (2020).

35. Brown RT*, et al.* Pharmacokinetics of Escalating Doses of Oral Psilocybin in Healthy Adults. *Clin Pharmacokinet* **56**, 1543-1554 (2017).

36. Halberstadt AL, Koedood L, Powell SB, Geyer MA. Differential contributions of serotonin receptors to the behavioral effects of indoleamine hallucinogens in mice. *J Psychopharmacol* **25**, 1548-1561 (2011).

37. Jefferson SJ*, et al.* 5-MeO-DMT modifies innate behaviors and promotes structural neural plasticity in mice. *Neuropsychopharmacology*, Online ahead of print (2023).

38. Torrado Pacheco A, Olson RJ, Garza G, Moghaddam B. Acute psilocybin enhances cognitive flexibility in rats. *Neuropsychopharmacology* **48**, 1011-1020 (2023).

39. Hibicke M, Landry AN, Kramer HM, Talman ZK, Nichols CD. Psychedelics, but Not Ketamine, Produce Persistent Antidepressant-like Effects in a Rodent Experimental System for the Study of Depression. *ACS Chem Neurosci* **11**, 864-871 (2020).

40. Cameron LP*, et al.* 5-HT2ARs Mediate Therapeutic Behavioral Effects of Psychedelic Tryptamines. *ACS Chem Neurosci* **14**, 351-358 (2023).

41. Hesselgrave N, Troppoli TA, Wulff AB, Cole AB, Thompson SM. Harnessing psilocybin: antidepressant-like behavioral and synaptic actions of psilocybin are independent of 5-HT2R activation in mice. *Proc Natl Acad Sci U S A* **118**, (2021).

42. Woodburn SC, Levitt CM, Koester AM, Kwan AC. Psilocybin Facilitates Fear Extinction: Importance of Dose, Context, and Serotonin Receptors. *ACS Chem Neurosci* **15**, 3034-3043 (2024).

43. Davoudian PA, Shao LX, Kwan AC. Shared and Distinct Brain Regions Targeted for Immediate Early Gene Expression by Ketamine and Psilocybin. *ACS Chem Neurosci* **14**, 468-480 (2023).

44. Nichols DE. Psychedelics. *Pharmacol Rev* **68**, 264-355 (2016).

45. Savalia NK, Shao LX, Kwan AC. A Dendrite-Focused Framework for Understanding the Actions of Ketamine and Psychedelics. *Trends Neurosci* **44**, 260-275 (2021).

46. Yao Z*, et al.* A taxonomy of transcriptomic cell types across the isocortex and hippocampal formation. *Cell* **184**, 3222-3241.e3226 (2021).

47. Zolnik TA*, et al.* Layer 6b controls brain state via apical dendrites and the higher-order thalamocortical system. *Neuron* **112**, 805-820 e804 (2024).

48. Schuman B, Machold RP, Hashikawa Y, Fuzik J, Fishell GJ, Rudy B. Four Unique Interneuron Populations Reside in Neocortical Layer 1. *J Neurosci* **39**, 125-139 (2019).

49. Krabbe G, Matyash V, Pannasch U, Mamer L, Boddeke HW, Kettenmann H. Activation of serotonin receptors promotes microglial injury-induced motility but attenuates phagocytic activity. *Brain Behav Immun* **26**, 419-428 (2012).

50. Kolodziejczak M*, et al.* Serotonin Modulates Developmental Microglia via 5-HT2B Receptors: Potential Implication during Synaptic Refinement of Retinogeniculate Projections. *ACS Chem Neurosci* **6**, 1219-1230 (2015).

51. Carson MJ, Thomas EA, Danielson PE, Sutcliffe JG. The 5-HT5A serotonin receptor is expressed predominantly by astrocytes in which it inhibits cAMP accumulation: A mechanism for neuronal suppression of reactive astrocytes. *Glia* **17**, 317-326 (1996).

52. Kim MC*, et al.* Method of moments framework for differential expression analysis of single-cell RNA sequencing data. *Cell* **187**, 6393-6410 e6316 (2024).

53. Chen Y, Lun AT, Smyth GK. From reads to genes to pathways: differential expression analysis of RNA-Seq experiments using Rsubread and the edgeR quasi-likelihood pipeline. *F1000Res* **5**, 1438 (2016).

54. Squair JW*, et al.* Confronting false discoveries in single-cell differential expression. *Nat Commun* **12**, 5692 (2021).

55. Murphy AE, Skene NG. A balanced measure shows superior performance of pseudobulk methods in single-cell RNA-sequencing analysis. *Nat Commun* **13**, 7851 (2022).

56. Takemoto-Kimura S*, et al.* Calmodulin kinases: essential regulators in health and disease. *J Neurochem* **141**, 808-818 (2017).

57. Schmitt JM, Guire ES, Saneyoshi T, Soderling TR. Calmodulin-dependent kinase kinase/calmodulin kinase I activity gates extracellular-regulated kinase-dependent long-term potentiation. *J Neurosci* **25**, 1281-1290 (2005).

58. Myers SJ, Yuan H, Kang JQ, Tan FCK, Traynelis SF, Low CM. Distinct roles of GRIN2A and GRIN2B variants in neurological conditions. *F1000Res* **8**, (2019).

59. von Engelhardt J*, et al.* CKAMP44: a brain-specific protein attenuating short-term synaptic plasticity in the dentate gyrus. *Science* **327**, 1518-1522 (2010).

60. Schmitz LJM*, et al.* The AMPA receptor-associated protein Shisa7 regulates hippocampal synaptic function and contextual memory. *Elife* **6**, (2017).

61. Arnold S. The power of life--cytochrome c oxidase takes center stage in metabolic control, cell signalling and survival. *Mitochondrion* **12**, 46-56 (2012).

62. Sanz-Morello B*, et al.* Complex IV subunit isoform COX6A2 protects fast-spiking interneurons from oxidative stress and supports their function. *EMBO J* **39**, e105759 (2020).

63. Holper L, Lan MJ, Brown PJ, Sublette EM, Burke A, Mann JJ. Brain cytochrome-c-oxidase as a marker of mitochondrial function: A pilot study in major depression using NIRS. *Depress Anxiety* **36**, 766-779 (2019).

64. Khadimallah I*, et al.* Mitochondrial, exosomal miR137-COX6A2 and gamma synchrony as biomarkers of parvalbumin interneurons, psychopathology, and neurocognition in schizophrenia. *Mol Psychiatry* **27**, 1192-1204 (2022).

65. Lee BC, Tsai JC, Huang YH, Wang CC, Lee HC, Tsai HJ. The 419th Aspartic Acid of Neural Membrane Protein Enolase 2 Is a Key Residue Involved in the Axonal Growth of Motor Neurons Mediated by Interaction between Enolase 2 Receptor and Extracellular Pgk1 Ligand. *Int J Mol Sci* **25**, (2024).

66. Haque A, Polcyn R, Matzelle D, Banik NL. New Insights into the Role of Neuron-Specific Enolase in Neuro-Inflammation, Neurodegeneration, and Neuroprotection. *Brain Sci* **8**, (2018).

67. Bandara AB, Drake JC, James CC, Smyth JW, Brown DA. Complex I protein NDUFS2 is vital for growth, ROS generation, membrane integrity, apoptosis, and mitochondrial energetics. *Mitochondrion* **58**, 160-168 (2021).

68. Dunham-Snary KJ*, et al.* Ndufs2, a Core Subunit of Mitochondrial Complex I, Is Essential for Acute Oxygen-Sensing and Hypoxic Pulmonary Vasoconstriction. *Circ Res* **124**, 1727-1746 (2019).

69. Phoumthipphavong V, Barthas F, Hassett S, Kwan AC. Longitudinal Effects of Ketamine on Dendritic Architecture In Vivo in the Mouse Medial Frontal Cortex. *eNeuro* **3**, ENEURO.0133-0115.2016 (2016).

70. Ng LHL, Huang Y, Han L, Chang RC, Chan YS, Lai CSW. Ketamine and selective activation of parvalbumin interneurons inhibit stress-induced dendritic spine elimination. *Transl Psychiatry* **8**, 272 (2018).

71. Moda-Sava RN*, et al.* Sustained rescue of prefrontal circuit dysfunction by antidepressant-induced spine formation. *Science* **364**, eaat8078 (2019).

72. de la Fuente Revenga M*, et al.* Prolonged epigenomic and synaptic plasticity alterations following single exposure to a psychedelic in mice. *Cell Rep* **37**, 109836 (2021).

73. Cameron LP*, et al.* A non-hallucinogenic psychedelic analogue with therapeutic potential. *Nature* **589**, 474-479 (2021).

74. Fanibunda SE*, et al.* Serotonin regulates mitochondrial biogenesis and function in rodent cortical neurons via the 5-HT(2A) receptor and SIRT1-PGC-1alpha axis. *Proc Natl Acad Sci U S A* **116**, 11028-11037 (2019).

75. Tullai JW, Schaffer ME, Mullenbrock S, Sholder G, Kasif S, Cooper GM. Immediate-early and delayed primary response genes are distinct in function and genomic architecture. *J Biol Chem* **282**, 23981-23995 (2007).

76. Hrvatin S*, et al.* Single-cell analysis of experience-dependent transcriptomic states in the mouse visual cortex. *Nat Neurosci* **21**, 120-129 (2018).

77. Tyssowski KM*, et al.* Different Neuronal Activity Patterns Induce Different Gene Expression Programs. *Neuron* **98**, 530-546 e511 (2018).

78. van den Brink SC*, et al.* Single-cell sequencing reveals dissociation-induced gene expression in tissue subpopulations. *Nat Methods* **14**, 935-936 (2017).

79. Lacar B*, et al.* Nuclear RNA-seq of single neurons reveals molecular signatures of activation. *Nat Commun* **7**, 11022 (2016).

80. Ding J*, et al.* Systematic comparison of single-cell and single-nucleus RNA-sequencing methods. *Nat Biotechnol* **38**, 737-746 (2020).

81. Nagy C*, et al.* Single-nucleus transcriptomics of the prefrontal cortex in major depressive disorder implicates oligodendrocyte precursor cells and excitatory neurons. *Nature Neuroscience* **23**, 771-781 (2020).

82. Zeng L*, et al.* A Single-Nucleus Transcriptome-Wide Association Study Implicates Novel Genes in Depression Pathogenesis. *Biol Psychiatry* **96**, 34-43 (2024).

83. Tran MN*, et al.* Single-nucleus transcriptome analysis reveals cell-type-specific molecular signatures across reward circuitry in the human brain. *Neuron* **109**, 3088-3103 e3085 (2021).

84. Virshup I, Rybakov S, Theis FJ, Angerer P, Wolf FA. anndata: Annotated data. *biorxiv*, (2021).

85. Wolf FA, Angerer P, Theis FJ. SCANPY: large-scale single-cell gene expression data analysis. *Genome Biol* **19**, 15 (2018).

86. Wolock SL, Lopez R, Klein AM. Scrublet: Computational Identification of Cell Doublets in Single-Cell Transcriptomic Data. *Cell Syst* **8**, 281-291 e289 (2019).

87. Nakao A, Yoshihama M, Kenmochi N. RPG: the Ribosomal Protein Gene database. *Nucleic Acids Res* **32**, D168-170 (2004).

88. Herring CA*, et al.* Human prefrontal cortex gene regulatory dynamics from gestation to adulthood at single-cell resolution. *Cell* **185**, 4428-4447 e4428 (2022).

89. McInnes L, Healy J, Melville J. UMAP: Uniform Manifold Approximation and Projection for Dimension Reduction. *biorxiv*, (2020).

90. Fischer S, Gillis J. How many markers are needed to robustly determine a cell's type? *iScience* **24**, 103292 (2021).

91. Tasic B*, et al.* Shared and distinct transcriptomic cell types across neocortical areas. *Nature* **563**, 72-78 (2018).

92. Hafemeister C, Halbritter F. Single-cell RNA-seq differential expression tests within a sample should use pseudo-bulk data of pseudo-replicates. *biorxiv*, (2023).

93. Chen EY*, et al.* Enrichr: interactive and collaborative HTML5 gene list enrichment analysis tool. *BMC Bioinformatics* **14**, 128 (2013).

94. Kuleshov MV*, et al.* Enrichr: a comprehensive gene set enrichment analysis web server 2016 update. *Nucleic Acids Res* **44**, W90-97 (2016).

95. Xie Z*, et al.* Gene Set Knowledge Discovery with Enrichr. *Curr Protoc* **1**, e90 (2021).